ADVANCED ENGINEERING MATERIALS

FULL PAPER

DOI: 10.1002/adem.201600130

High-Performance Multifunctional Thermoplastic Composites Enhanced by Aligned Buckypaper**

By *Zhongrui Li,* Jin Gyu Park* and *Zhiyong Liang*

High-performance lightweight composites are sizably manufactured by impregnating continuous aligned carbon nanotube sheet (buckypapers) with self-reinforcing polyphenylene (Parmax) solution and followed by hot-press. The high processing pressure flattens nanotubes, which preferably π-stack with the aromatic rings of Parmax chain, and accordingly improve the load transfer. Both tensile strength and Young's modulus of the thermoplastic composites increase with the alignment degree of nanotubes, and can reach 950 MPa and 94 GPa, respectively, for the composite containing 50%-stretched buckypaper. The highly aligned nanotubes also boost phonon transfer (70 W mK^{-1}) and the electric conductivity (425 S cm^{-1}) of the composite along the alignment direction. These combined outstanding properties would enable the thermoplastic composites in wide applications as multifunctional material.

1. Introduction

Compared with thermosets, the thermoplastics offer several exciting features including excellent recyclability, better toughness, unlimited shelf-life, and rapid fabrication cycle. Recently, a novel family of processable self-reinforced polyphenylenes (Parmax SRPs) was designed by carefully choosing pendant side chains to impart solubility and thermal processability to the normally intractable rigid-rod poly-paraphenylene backbones.[1] As a self-reinforced liquid crystalline copolymer of para-linked benzophenone and meta-linked unsubstituted phenylene units, Parmax possesses many properties superior to other thermoplastics, such as extraordinary strength, modulus, hardness, light density, outstanding thermal stability, and other properties in a combination unrivaled by any other single material.[2] For instance, the tensile strength of neat Parmax is approximately 207 MPa, and its tensile modulus can be above 5.5 GPa,[3] the highest among thermoplastics. More importantly, Parmax can be dissolved in numerous organic solvents (esters, N-methylpyrrolidinone, methylene chloride, phenyl ethers, etc.), and can be thermally fabricated (compression molded, injection molded, extruded, etc.). However, the tensile strength of Parmax itself still needs to be improved for such applications as aerospace. Additionally, its poor charge transport, low Seebeck coefficient, and thermal conductivity excluded it in the uses as thermoelectric materials or conductors.

As a novel type of one-dimensional inorganic materials, carbon nanotubes (CNTs) bring many hopes in the fabrication of multifunctional composites because individual CNTs possess a combination of excellent properties, including superlative mechanic strength, remarkable charge transport, and thermal conductivities. CNTs can be viewed as one or several graphitic sheets of sp^2 hybridized carbon atoms wrapped into a tube. This σ-bonding structure provides CNTs with unique axial strength and extremely high thermal conductivity (theoretically up to 6 600 W (m-K)$^{-1}$).[4] CNTs are the strongest known material in term of tensile strength.[5] Single-walled carbon nanotubes demonstrate an average breaking tensile strength of 30 GPa and Young's modulus of above 1 TPa.[6] The π-bonds perpendicular to the tube surface are responsible for the weak interaction between tubes in a bundle and the electrical transport properties. With very small diameters at nanometer scale, CNTs may reach very high

[*] *Dr Z. Li*
Electron Microbeam Analysis Laboratory (EMAL), University of Michigan, Ann Arbor, Michigan 48109, USA
E-mail: zhongrui@umich.edu
Dr Z. Li, Dr. J. G. Park, Dr. Z. Liang
High Performance Material Institute (HPMI), Florida State University, Tallahassee, Florida 32310, USA

[**] *This research is supported by ONR (N00014-11-1-0274) project. The sponsorship and oversight of the program by Dr. Ignacio Perez are greatly appreciated. The authors would like to acknowledge Rebekah Downes for stretching buckypaper and Dr. Shaokai Wang for the assistance of thermogravimetric analysis. The fitting software Smartfit used for Raman analysis was provided by Dr. Wei Zhou. The thermal and electrical conductivities of the composites were measured on Dr. Jun Lu's Physical Property Measurement System (PPMS, Quantum Design) at the National High Magnetic Field Laboratory.*

ADVANCED ENGINEERING MATERIALS

aspect ratios of 1 000 and beyond. Plus the large surface area ($\sim$1 000 $m^2 g^{-1}$), all these make CNTs ideal fillers for polymers to enhance their performances.

However, the outstanding properties of individual tubes do not ensure the high performance of the resulting composites due to low volume fraction, phase separation, short tube length, random orientation, wall defects, and weak interfacial load transfer.[7] Previously, the tensile performance of composites (less than 10 wt% of CNT loading) is described using a single volume fraction, which leads to a series of errors.[8] Additionally, the essence of the tube orientation distribution is often simplified to one parameter, Krenchel's orientation efficiency factor, η_o,[9,10] i.e., the modulus and strength of composites filled with rod-like fillers are proportional to η_o.[11] However, the Cox–Krenchal rule of mixtures has not been fully validated for a wide range of orientations (i.e., η_o value ranges from 0 to 1) for any nanocomposite.[12] It remains unclear whether continuum theory is valid at the molecular scale.

Inspired by nacre (mother of pearl), which consists of high inorganic content (almost 95 vol% calcium carbonate) and low-elastic biopolymers, possesses remarkable strength and toughness thanks to its hierarchical structure and precise inorganic–organic interface, we fabricated sizable high-performance thermoplastic composites from a flattened CNT sheets (buckypaper) and self-reinforcing polyphenylene (Parmax) by a solution and hot-press approach. Buckypaper is a form of two-dimensional sheet of CNTs of different length and diameter, very suitable for practical macroscale applications. To improve the tube interaction and alignment, buckypaper sheets are first stretched and used for composite fabrication as shown in Figure 1. The nanotube weight fraction or loadings are controlled at around 55 wt% in the composite samples for the optimal interaction between tubes and polymer through a solution impregnation process. The high-processing pressure facilitates the interfacial interaction between the flattened nanotubes and aromatic rings of the polymer; as a result, the macroscopic lightweight buckypaper/Parmax composites demonstrate outstanding mechanical, thermal, and electrical properties, ensuring a broad range of multifunctional applications.

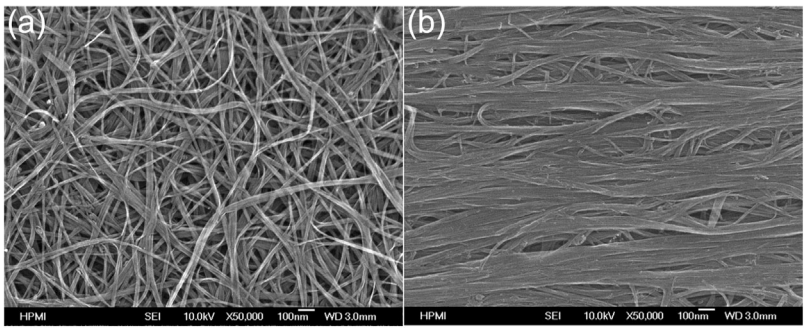

Fig. 1. SEM images of pre-stretched (a) and 50%-stretched (b) buckypaper.

2. Results and Discussion

2.1. Morphology, Structure, and Mechanical Properties of Differently Stretched Buckypapers

Generally, the performances of buckypapers are still not as good as those of individual CNTs, mainly due to the weak interface interactions between tubes in the buckypaper, as compared to the chemical bonds in the individual tubes. The crookedness and agglomeration of the CNTs remarkably reduce the mechanical strength[13] and the thermal conductivity[14] of the buckypapers. One of the critical issues that prevent the full utilization of strengthening potential of CNTs is their waviness and random orientation. Randomly oriented wavy CNTs do not carry the load at the same time, are loosely packed, and have weak tube–tube contacts, all of which are not beneficial to the strength, stiffness, and electrical and thermal conductivities of resulting composites. The alignment of the nanotubes directly affects many physical properties of the resulting composite, including mechanical strength, thermal and electrical conductivities. We started from the randomly dispersed CNT sheets (purchased from Nanocomp Technologies Inc., Concord, NH), in which CNTs are hundreds of micrometer-long and small-diameter (3–8 nanometers) with 2–5 walls. The nanotubes in the buckypaper sheets are substantially entangled and possibly interconnect each other through floating catalyst particles and aero-gel.[15] The commercially available buckypapers can reach up to several meters long, which enables them suitable for manufacturing composites at large scale. Alignment of CNTs in buckypaper can be realized through stretching. As seen from the tensile test below (see Figure 3), the pristine buckypaper can be directly stretched up to 24% before break. Note that large length of tubes in the buckypaper is crucial for the success of large stretching ratio, i.e., high alignment of tubes in the buckypaper. With millimeter long tubes, Chen et al. successfully stretched the buckypaper up to 40% without break.[16] For our relatively short-tube buckypaper, in order to get even higher alignment, say 50% stretching, a resin (Hexcel 8552 agent) is first added into the randomly dispersed buckypaper to make prepreg, and stretched it under infrared heating. After then the agent is removed from the buckypaper by acetone solvent washing (the agent residual on the resulting buckypaper is less than 0.5 wt% as revealed by the thermogravimetric study). The integrity of these CNT films maintain through Van der Waals forces and entanglement interactions among the CNTs. This approach can stretch sheet up to 50% longer than the pre-stretch sheet. Figure 1 shows the morphologies of the pre- and post-stretched buckypaper samples. Compared to the reported magnetic alignment in neat CNT sheet[17] and solid-state drawing from synthesized CNT arrays,[18] our wet-stretching approach can reach macroscopic size at much lower cost.[19]

To evaluate the effects of the stretching on the degree of the alignment, wide angle X-ray scattering (WAXS) and polarized Raman scattering measurements were carried out to determine the degree of the CNT alignment.[20] Multi-wall carbon nanotubes (MWNTs) exhibited a wide-angle feature around 27° arising from diffraction from the layered graphene sheets (interlayer spacing d). For 1D MWNTs with a large aspect ratio, this feature is similarly restricted in reciprocal space to a thin plane perpendicular to the nanotube axis, leading to diffraction spots in the wide-angle regime, which also become azimuthally spread out in the presence of a distribution of MWNT orientation (inset of Figure 2a). A characteristic of X-ray patterns from a uniaxial oriented MWNT strip is the paired arcs showing a narrow distribution with respect to the azimuth chi (χ) circle of the incident beam. The azimuthal width of the arcs directly reflects the alignment degree of the tubes. The width of Bragg arc shrinks with an increasing stretch ratio (Figure 2a). The full-width at half-maximum of the azimuthal peak decreases from 52.1° for the 15%-stretched buckypaper, to 25.8° and 19.3° for 35- and 50%-stretched buckypapers, respectively. In the wide-angle scattering patterns recorded in this study, a strong background scattering results from the impurities such as amorphous carbon, catalyst particles. The azimuthal angle (χ) dependence includes both Bragg and diffuse scattering from crystalline and noncrystalline components, respectively, in some unknown ratio. It would overestimate the unaligned part of MWNTs in the network if Hermans orientation function is calculated directly using the X-ray diffraction diagram.[21] After the background removal and peak area normalization, the tube number distribution around the orientation can be directly read out from the Bragg arc intensity of a narrow θ-range only containing the MWNT diffraction peak, and the Herman's orientation parameter were calculated: $S_d = (3\langle\cos^2\chi\rangle - 1)/2$, where $\langle\cos^2\chi\rangle = \left(\int_0^{\pi} I(\chi)\sin\chi\cos^2\chi d\chi\right) / \int_0^{\pi} I(\chi)\sin\chi d\chi$.

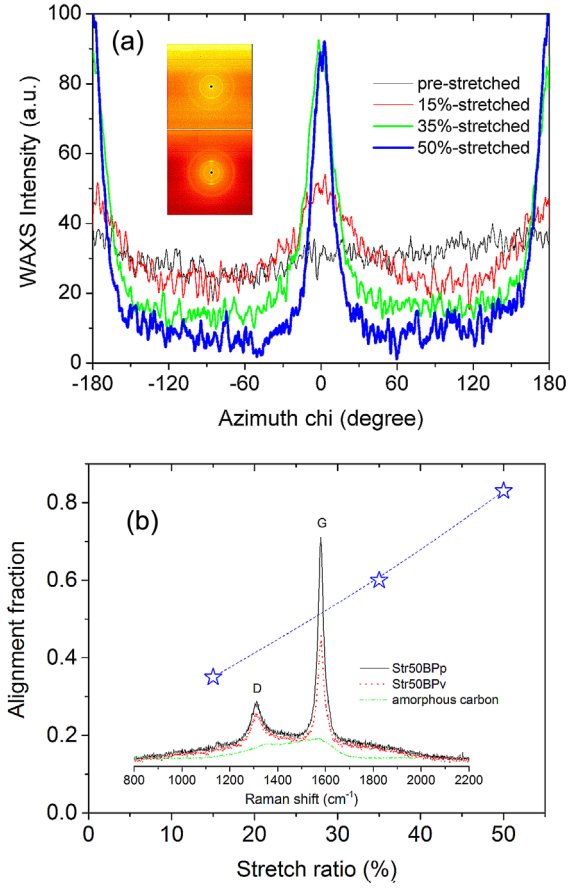

Fig. 2. (a) Integrated 2D X-ray scattering intensity (summed over intervals $24° < 2\theta < 30°$) displaying the azimuth peaks for nanotubes in the differently stretched buckypaper samples. The inset displays 2D X-ray scattering pattern images of (inset up) the pre-stretched and (inset bottom) 50%-stretched buckypaper. (b) The alignment fractions estimated from G band intensities at orientation angle between stretching direction and laser polarization. The inset of (b) displays the Raman spectra of 50% stretched buckypaper collected at the electric field parallel (Str50BPp) and perpendicular (Str50BPv) to the alignment direction, along with that of amorphous carbon.

It turns out that S_d is roughly proportional to the stretch ratio. The calculated values of Herman's orientation parameter S_d for the buckypaper strips are 0.01, 0.27, 0.61, and 0.86 for the strains of 0, 15, 35, and 50%, respectively.

G-band (≈1 590 cm^{-1}) Raman scattering intensity of carbon nanotube is sensitive to the orientation of the tube axis with respect to the electric polarization vectors of the excitation laser beam (the inset in Figure 2b). A distribution function of tube axis orientations can be obtained by exciting CNTs with a polarized laser beam and collecting G-band scattering intensity at different angles between the preferred axis and VV polarization vector. The G-band Raman intensity of an oriented CNT changes with $\cos^4\theta$, where θ is the angle between the incident excitation polarization and the CNT axis (in the plane perpendicular to the Poynting vector of the incident excitation).[22] Due to the anisotropicity of optical absorption in CNT,[23] the orientation dependence of the penetration depth may be corrected by a correction factor $f_{abs} \approx 1/(cos\theta + Ksin\theta)$, where $K = a_\perp/a_\parallel$, $a_\perp$ and $a_\parallel$ are the absorption coefficients of CNTs for polarizations perpendicular and parallel to the tube axis, respectively. K is estimated to be in the range from 0 to 0.25.[24] The axially symmetricity of CNTs renders the distribution function a Gaussian cylindrical symmetry. In principle, aligned fraction η and FWHM can be obtained by fitting the deviation from a $f_{abs}\cdot\cos^4\theta$ law. The out-of-plane Raman scattering intensity is much less than the in-plane misalignment when the polarization vector of the laser lies in-plane, so the alignment fractions from 2D and 3D models differs by only a few percent. For our thin buckypaper sheets (10–45 μm), we use a 2D model by neglecting the anisotropic optical penetration depth,[25] the deviation from perfectly (100%) aligned buckypaper can be quantified by fitting the Raman intensity curves with the following expression:

$$I(\theta,\eta,\sigma) = A\int_0^{\pi/2}\left[\frac{1-\eta}{\pi} + \frac{\eta}{\sigma\sqrt{\pi/2}}e^{-2(\phi-\theta)^2/\sigma^2}\right]\cdot\frac{\cos^4\phi}{\cos\phi + K\sin\phi}d\phi,$$

where η and σ are the alignment fraction and the Gaussian standard deviation (equivalent FWHM $=\sigma\sqrt{2\ln 2}$), respectively. The intensity ratio for two orthogonal measurements at $\theta=0$ and $\pi/2$ depends on both σ and η. If σ is small, η can be given from $I(0)/I(\pi/2)$. Note that the depth sampled by Raman scattering in the weakly absorbing transverse orientation $\theta=\pi/2$ is greater than that in $\theta=0$, which leads to $I(\pi/2)$ is overestimated relative to $I(0)$, so η is underestimated (and/or σ is overestimated). Generally, only with very accurate Raman intensities taken at many θ's, σ can be obtained by fitting the deviation from a $\cos^4\theta$ law. It inherently limits the Raman method in the accurate determination of CNT alignment degree as compared to X-ray scattering diagrams. Background correction is performed by subtracting a Raman spectrum of amorphous carbon. Then, the alignment degree can be obtained from the best fitting curve of the Raman intensity versus orientation angle. The estimated values are 0.35, 0.60, and 0.83 for the 15-, 35-, and 50%-stretched buckypaper strips, respectively, with a uncertainty of ± 0.05.

The tensile properties of the neat (i.e., without polymer) buckypaper strips of different stretch ratios were measured and displayed in Figure 3a. The randomly dispersed buckypaper (*rndmBP*) exhibits the mechanical strength at breakage and Young's modulus of approximately 119 MPa and 1.5 GPa, respectively. Load carrying along the alignment direction shows significant improvements for the stretched buckypaper specimens. As seen from Table 1 and Figure 3a, the tensile strength of the buckypaper strips nearly linearly increase with the orientation factor, and reaches to 383 MPa for the 50%-stretched buckypaper samples, about 221% improvements over the *rndmBP*. The Young's modulus of the post-stretched buckypaper strips show even more dramatic improvements along the alignment direction, from 1.5 GPa for the randomly dispersed (pre-stretched) sheet to 16.2 GPa for *Str50BP*.

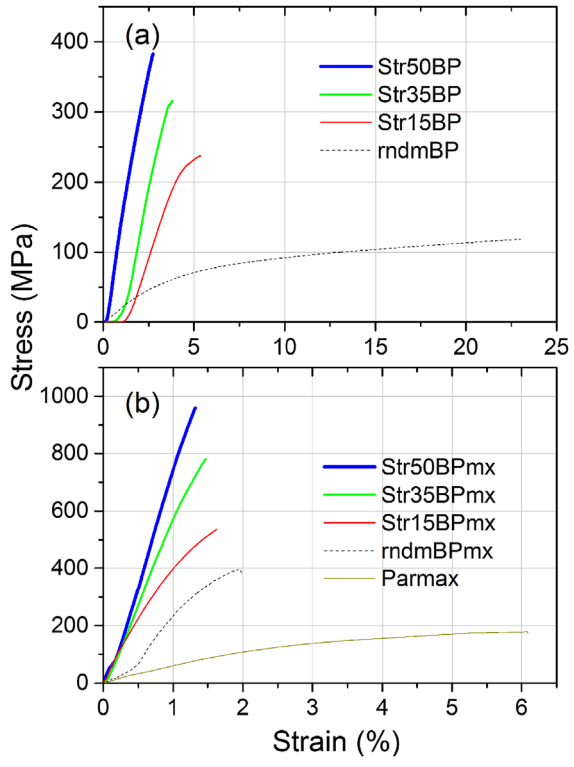

Fig. 3. The typical uniaxial tensile stress–strain curves of the differently stretched buckypaper strips (a) and the stretched buckypaper/Parmax composites (b) along the nanotube alignment direction.

Table 1. Tensile mechanical performances of the differently stretched buckypaper strips and the stretched buckypaper/Parmax composites (b) along the nanotube alignment direction. Parmax is also listed for comparison.

Sample name	Young's modulus [Gpa]	Tensile strength [MPa]	Elongation at break [%]	Density [g cm^{-3}]
rndmBP	1.5 ± 0.2	119 ± 7	23.9 ± 4.2	0.81 ± 0.05
Str15BP	7.8 ± 0.6	237 ± 21	5.4 ± 1.1	0.82 ± 0.05
Str35BP	12.5 ± 1.1	315 ± 28	3.8 ± 0.8	0.84 ± 0.05
Str50BP	16.2 ± 1.4	383 ± 35	2.8 ± 0.7	0.85 ± 0.05
Parmax	3.8 ± 0.3	178 ± 16	6.1 ± 1.3	1.14 ± 0.05
rndmBPmx	29.1 ± 2.7	384 ± 35	2.0 ± 0.9	1.21 ± 0.05
Str15BPmx	52.1 ± 4.5	535 ± 48	1.7 ± 0.7	1.11 ± 0.05
Str35BPmx	75.3 ± 6.3	780 ± 70	1.5 ± 0.6	1.02 ± 0.05
Str50BPmx	93.8 ± 8.1	958 ± 86	1.3 ± 0.5	0.98 ± 0.05

Compared to other nanotube sheets,[26,27] the CNTs in our buckypapers have a much larger aspect ratio ($\approx 10^5$), which results in more entanglements that maintain the integrity of the nanotube networks during the stretching process. Along the load direction the waviness of the CNTs get straightened, CNTs in buckypaper tends to the self-assembling and denser packing of the CNT bundles[28] which significantly improve the load carrying and transfer of the aligned nanotubes in the axial tensile direction, dramatically improving the mechanical tensile properties. In the most cases where CNTs are shorter than the gauge length, the Young's modulus of a buckypaper can be empirically expressed as:

$$Y=\eta_o\eta_l f Y_{tt},\qquad f=\frac{f_v+f_v^2}{2}, \tag{1}$$

where η_o and η_l are the correction factors (ranging from 0 to 1) for the effects of nanotube orientation and length, respectively. Y_{tt} is the CNT modulus. Since, the load transfer mainly works through the interfacial interaction between the tubes, instead of directly using tube volume factor f_v, an interpolating factor f is introduced into the equation ($1-f_v$ is the nanoporosity or the fraction of the void space inside the buckypaper), just similar to the model proposed by Lielens et al. that interpolates between the upper and lower bounds.[29]

According to Alan H. Windle's model,[30] the axial stress in the CNT bundles results from stress transfer between adjacent tubes through shear, which monotonically increases with the CNT length. For given length of tubes, a high degree of contact between the rigid neighboring tubes and load-transfer

efficiency can be realized by maximizing alignment of nanotubes in buckypaper.[31] The enhanced densification and orientation of CNTs can improve the tensile strength, thermal and electrical conductivities of the buckypaper.[32] A small reorientation of nanotubes to the aligned direction may be attributed to the increase of van der Waals forces between the aligned individual nanotubes, since the van der Waals force strongly depends on the distance between nanotubes. Consequently, their tensile performances get high. The buckypaper typically breaks because of CNT pullout, tube/tube sliding, de-bundling, telescoping of MWNTs, and delamination between layered structures.

2.2. Mechanical Properties, Electrical, and Thermal Conductivities of Buckypaper/Parmax Composites

2.2.1. Tensile Properties of the Composites

Figure 3b shows the typical uniaxial tensile stress–strain curves of the differently stretched-buckypaper/Parmax composites along the nanotube alignment direction. The Young's modulus and tensile strength for the neat Parmax are around 3.8 GPa and 178 MPa, respectively. As shown in Figure 3b, the incorporation of CNTs into Parmax improves the tensile properties compared to the neat polymer. The randomly dispersed buckypaper/Parmax composite (the control sample, *rndmBPmx*) exhibit a tensile strength of approximately 300 MPa, and the Young's modulus of 29.1 GPa.

The tensile strength and Young's modulus measurements of the samples are summarized in Table 1 to show the buckypaper stretching effects on the mechanical performances of the composites. After incorporating Parmax polymer onto the aligned buckypaper, the resulting stretched buckypaper/Parmax composites demonstrate dramatically increased tensile performances. However, as a direct indicator of a material's toughness, the elongation at break decreases sharply with the CNT alignment, because the strong interfacial stress increasingly restrict the mobility of Parmax molecular chain.[33] The 15%-stretched buckypaper/Parmax composite (*Str15BPmx*) demonstrates a tensile strength and a Young's modulus of 571 and 52.1 GPa, respectively. For the stretched buckypaper/Parmax composites, both the tensile strength and Young's modulus monotonically increase with the orientation fraction of the CNTs in the stretched buckypaper. As the CNT alignment further increases by stretching the buckypaper 50%, the Young's modulus and tensile strength of the 50%-stretched buckypaper/Parmax composite (*Str50BPmx*) reach up to about 22 times (94 GPa) and 5 times (958 MPa), respectively, relative to those of the neat Parmax. These values are also 5.8 and 2.5 times of those of the 50%-stretched buckypaper (*Str50BP*). Additionally, the buckypaper/Parmax composites have a very light mass density ($\approx 1\,g\,cm^{-3}$), hence the buckypaper/Parmax composites are highly competitive as compared with most structural metals and many thermoset composites.

The stretched-buckypaper composites contain more aligned and straight nanotubes (Figure 4a), which consequently lead to the reduced gaps and the improved tube contacts. Most of nanotubes in the composite are aligned in the axial tensile direction, which are also shown in the cross-sectional fracture after tensile testing (Figure 4b). The incorporation of Parmax into the aligned buckypaper frame enhances the interfacial bonding between the Parmax chain and the nanotubes.[34] Taking the 50%-stretched buckypaper/Parmax composites (*Str50BPmx*) as example, the alignment degree of the CNTs in the composite along the axial direction is around 0.81, indicating that most nanotubes aligned along the stress direction carry a load under the tensile stress.

Interfacial bonding between the CNTs and Parmax chain also plays an important role in the improved tensile performance of the composites. The CNTs are peeled off from the fracture, while Parmax chain is believed to coat on the nanotube bundle surface as high nanotube concentration and no bulk neat polymer fractures are observed (Figure 4b), suggesting the good dispersion quality and the reinforcing mechanism of the CNTs. Many stretch deformations of the buckypaper/Parmax sheets are present, indicating effective load transfer between the CNTs and Parmax in the composites. The strong interfacial adhesion between the CNTs and Parmax allows for improved load transfer from the polymer to the nanotubes.[35] The CNTs are pulled out from the composites and become very stretched strips with obvious diameter change with sharp breaks at the end due to CNT slippage within the bundles. Furthermore, although the resultant composites showed high tensile strength, almost no broken individual nanotubes are seen – clear evidence that the full potential of CNTs' strength has yet to be completely realized. Further improvements in interfacial bonding and load transfer should be able to reach a much higher level of mechanical performance.[36]

It is also worth mentioning that during the compounding process, the CNTs and their assemblages underwent collapse, flattened packing, preferred stacking, folding, and twisting

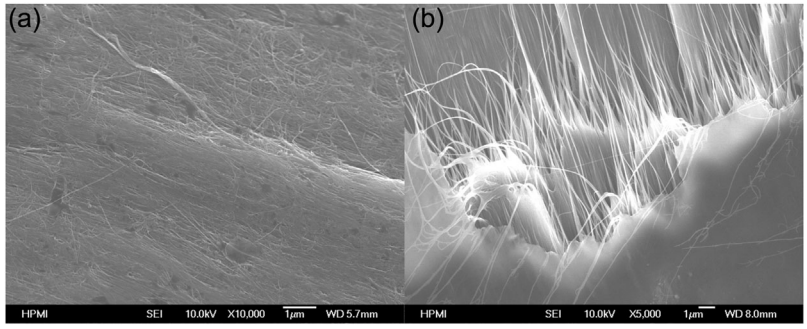

Fig. 4. (a) A composite sheet stretched by 50%, showing straight, well-aligned and closely packed nanotubes. (b) The SEM image of typical fracture surface morphology of buckypaper/Parmax composites with a 50%-stretch ratio. Stretched deformation of CNT array along stress direction suggests good alignment and load transfer. High volume fraction, good matrix penetration, and a layered failure mode are observed for all of the composites.

ADVANCED ENGINEERING MATERIALS

under a very high pressure (2 MPa).[37] The flattened CNTs are well packed into one layer along the alignment direction, working as do the layers inside nacre. The flattened nanotubes preferably π-stacking interact with the aromatic rings of Parmax, which is good for both load transfer and phonon transport.[38] Thus, a combination of high loading of ultra-strong flattened CNTs and the hierarchical nano-/micro-structures remarkably enhance the mechanical and thermal performance of thermoplastic composites.

The tensile performance of buckypaper/Parmax composites increases with increase in the alignment degree of CNTs in the buckypaper frame, and the optimal CNT content for the tensile strength seems appear around 55 ± 10 wt%. In the process of tensile test, the individual nanotube and polymer chain in the Parmax/BP composites might not break and their lengths are much shorter than the gauge length. Additionally, there exists the strong interfacial interaction between the Parmax polymer chain and CNTs, so the simple mixture model for low fiber concentration composites does not apply here.[39] The tensile performance of the Parmax/BP composites stems from the interfacial interactions of tube-polymer (σ_{tp}), tube–tube (σ_{tt}) and polymer–polymer (σ_{pp}). The modulus (Y) and tensile strength (σ) of the thermoplastic composites can be approximated as:

$$\begin{aligned} Y &= \eta_o \eta_{lY} f Y_{tt} + \eta_o f(1-f) Y_{tp} + (1-f) Y_{pp} \\ \sigma &= \eta_o \eta_{l\sigma} f \sigma_{tt} + \eta_o f(1-f) \sigma_{tp} + (1-f) \sigma_{pp}, \end{aligned} \quad (2)$$

The $f(1-f)$ term in the Equation set 2 takes into account the interaction among inclusions and the effect of the free boundary of the specimen.[40] The length effect might take different forms for the modulus and strength: η_{LY} and $\eta_{L\sigma}$.[41] The Equation set 2 can hold for the composites with any CNT/Parmax volume ratio, i.e., the interpolation factor can range from 0 (pure Parmax) to 1 (pure buckypaper). In the case of pure buckypaper where $Y_{tp} = Y_{pp} = 0$, and $1-f$ can be treated as the nanoporosity of buckypaper, just like in the Equation 1. Additionally, the Equation set 2 might also apply in other composite systems with CNT aggregation.

2.3. Thermal and Electrical Conductivities of the Stretched Buckypaper/Parmax Composites

The temperature dependence of the thermal conductivity of the pre-stretched and 50%-stretched buckypaper/Parmax composites (*Str50BPmx*) is displayed in Figure 5a. The log–log plot of temperature-dependent thermal conductivities of the composites in the inset of Figure 5a is similar to quadratic ($\kappa \approx T^n$, $n = 1.7$–2.1), characteristic of the two-dimensional phonon distribution like in graphite.[42] The thermal conductivity typically increases parabolically at the low-temperature range, and linearly at medium-temperature range and saturates at room temperature. Above 150 K, the thermal conductivity of the composites either linearly or sublinearly increase with temperature, similar to that of the magnetic-field-aligned CNT-polymer composites,[43] due to the start of Umklapp process from anharmonic phonon–phonon scattering.

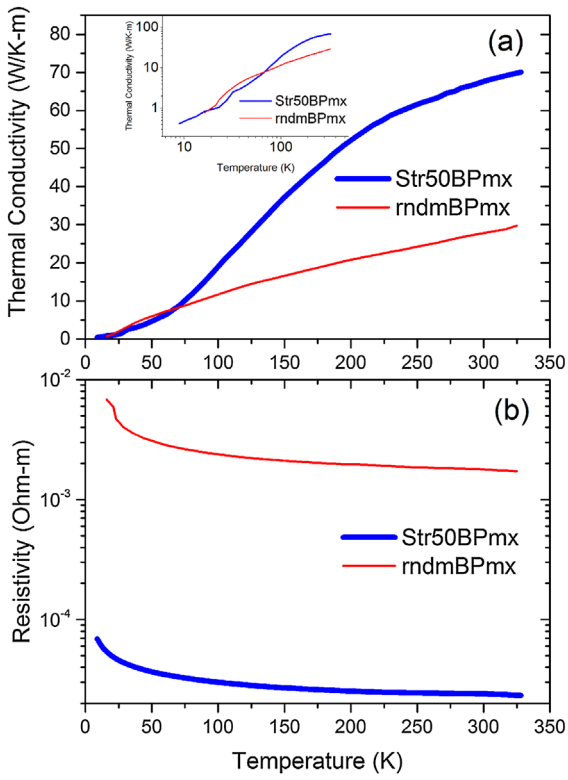

Fig. 5. (a) Temperature dependence of thermal conductivity of random and 50%-stretched buckypaper/Parmax composite. Inset is log–log plot of the thermal conductivity. (b) The resistivities of the random and 50%-stretched buckypaper/Parmax composite as a function of temperature.

The anharmonic phonon–phonon (or electron–phonon) scattering process creates a third phonon with a momentum k-vector outside the first Brillouin zone. The Umklapp process (flip-over) process limits the thermal conductivity of crystals, while the other normal phonon scattering occurs on crystal defects and at the sample surface. At very low temperatures, the Umklapp scattering are rare due to the tiny momentum of most phonons. At higher temperatures, the reduced radiation from the surface and onset of the Umklapp process result to the saturation of thermal conductivity. At room temperature, the thermal conductivity of *Str50BPmx* increases up to 70 W mK^{-1} along the alignment direction, which doubles that of the random sample (30 W mK^{-1}). The improved thermal conductivity of *Str50BPmx* are attributed to the alignment of CNTs, which leads to better intertube contacts between aligned CNTs in the buckypaper composite and increase the length and size of the CNT bundles, since the Parmax is a poor thermal conductor as compared to CNTs while the phonon/thermal transport mainly occur through CNT network. The best aligned buckypaper has better contact between nanotubes, resulting in better thermal conductivity. Additionally, the thermal boundary resistance at CNT–CNT contacts strongly affects heat transport across the composite due to the different alignment and continuity of the CNTs throughout the bundles.

Note that thermal interface between nanotubes and medium also plays an important role in the thermal

conductivity of the composites.[44] The low thermal interfacial resistance (R_K) can benefit high thermal conductivity. The Parmax fills the empty space in thin sheet between the CNTs act as a phonon transport medium. Therefore, the better CNT–CNT thermal contact and the CNT–Parmax interface is crucial to high thermal conductivity of CNT composites. The phonon mismatch at boundaries of the nanotube and Parmax results in high thermal boundary resistance (Kapitza resistance, R_K), and the phonon mode of CNTs can be altered by surrounding Parmax as a strain.[45] It is worth mentioning that since the inner shells of MWNTs can efficiently conduct phonons despite the outer shell interacting with the polymer matrix, MWNTs dispersed in polymer can enhance the thermal conductivity much more than single wall carbon nanotubes do.[46]

Since the stretched buckypapers demonstrate the dramatically increased tensile performances along the alignment direction, the better alignment, longer bundles, denser packing (less porous), and better contacts among the CNTs of the stretched buckypaper is expected to improve its electrical conductivity.[47,48] Along with thermal conductivity, the 2-probe electrical resistivity of the random and 50%-stretched buckypaper/Parmax composites are simultaneously measured as a function of temperature (Figure 5b). Parmax is a poor conductor with an electrical resistivity of approximately $10^{15}\,\Omega\,m$. As a polymer filler, CNT networks in buckypapers can naturally offer excellent charge transport paths for conductive composites due to their high electrical conductivity and high aspect ratio. The dispersion and alignment of CNTs in the polymer matrix are critical to determine the charge transportability of the polymer composites.[49] Despite the metallic origin of individual CNTs, the buckypaper composites show a negative temperature coefficient of resistance, $dR/dT < 0$. As seen in Figure 5b, the electrical resistivity of composite is dramatically reduced by the incorporation of buckypaper into Parmax in the whole temperature range. The pre-stretched buckypaper composite exhibits the resistivity of 17.2 $\Omega\,m$ at room temperature,[50] like typical carbon fiber composites.[51] Additionally, the electrical resistivity of the stretched-buckypaper/Parmax composites is significantly lower along the alignment direction of the CNTs than that of the pre-stretched buckypaper composite (*rndmPBmx*). When the 50%-stretched buckypaper is incorporated into the Parmax matrix, the resistivity of the composite drops to $2.35 \times 10^{-5}\,\Omega\,m$, about 7 orders of magnitude lower than that of *rndmPBmx*. The electrical conductivity (σ) of *Str50BPmx* is comparable to the aligned neat single wall carbon nanotube buckypaper.[52]

The high electric conductivities of the stretched buckypaper composites also stem from the CNT alignment and the dense packing of nanotubes. The better contacts among the nanotubes and longer tube bundles provide the more efficient percolation paths. Additionally, high concentration of CNTs in the composites and submillimeter-long CNTs can benefit the charge transport in the alignment direction. Moreover, with the Parmax smectic morphology the highly aromatic Parmax molecular chain forms the strong "π-stacking" with the flattened CNT walls which forms during the hot-press process.[53] Therefore, the intermolecular overlap π-stacking is indicated by good wetting and adhesion of CNTs with Parmax, i.e., a strong interaction and compatibility between the CNTs and the polymer matrix. Note that the highly aligned buckypaper/Parmax samples exhibit a larger anisotropic electrical conductivity than the thermal conductivity, because Parmax polymer is slightly thermally conductive but electrically insulating.

By testing the thermal and electrical conductivities of a composite, the electronic contribution to its thermal conductivity can be determined. According to Wiedemann–Franz law, Lorenz ratio $\kappa/\sigma T$, for metal in which free electrons get involved in both thermal and electric conductivities, is usually in the order of $10^{-8}\,W\Omega\,K^{-2}$. The Lorenz ratio does not vary much from metal to metal because the moving electrons transport both heat and a charge. The Lorenz ratio is in the order of $7–16 \times 10^{-5}\,W\Omega\,K^{-2}$ for the random buckypaper/Parmax composites and $1–2 \times 10^{-6}\,W\Omega\,K^{-2}$ in the composite *Str50BPmx* at various temperatures, essentially independent of temperature. These values are comparable to the previous measurements on carbon nanotube films, but two or three orders higher than expected for electron transport.[54,55] Thus, thermal conductivity is dominated by phonons at all temperatures, which might be interpreted with Tomonaga–Luttinger liquid theory for one-dimensional materials,[56] instead of the Fermi liquid theory for three-dimensional materials like bulk metal.

3. Conclusion

Wrapping up, highly aligned CNT sheets can be obtained by mechanically stretching buckypaper, and further impregnated with self-reinforcing polyphenylene (Parmax) to make high-performance thermoplastic composites with outstanding thermal, mechanical, and electrical properties. The wet impregnation approach provides a highly dispersed Parmax on the aligned CNT frame. The π-stacking between the highly aromatic Parmax chain and the flattened CNT wall leads to the strong interfacial interactions, and wetting and adhension between the polymer and CNTs in the buckypaper composites. With the incorporation of 50%-stretched buckypaper, the tensile strength and modulus of the composite improved by about 5 and 24 times, respectively, as compared to those of neat Parmax. The improved tensile performances are primarily attributed to strong interfacial interaction between the CNTs and Parmax, and the high-degree alignment of the millimeter long CNTs in the composite. An empirical expression was introduced to explain the influence of the orientation, length, and volume factors on the tensile performance of the buckypaper-enhanced thermoplastic composites with any CNT/polymer ratio by considering the interfacial interactions between the constitutes.

The high alignment degree of buckypaper also facilitate the high-thermal conductance and electrical conductivity of the

thermoplastic composites along the aligned direction. The 50%-stretched buckypaper/Pamax composite demonstrates 70 W mK^{-1} of thermal conductance and 425 S cm^{-1} of electric conductivity. Even higher performances of aligned buckypaper/Parmax composites are expected by optimizing the CNT-Parmax interface alignment and using much longer CNTs. The synthesis of foot-long CNTs is underway in our laboratory. Our approach can be easily scaled up for mass production of this kind of high performance thermoplastic composites. The combined outstanding performance of high mechanical properties and unprecedented electrical conductance enable the buckypaper/Pamax thermoplastic composites for a wide range of multi-functional/structural applications as lightweight composite conductors.

4. Experimental Section

4.1. Materials

The buckypapers are randomly dispersed MWNT sheets (Lot Number 4371, named as *rndmBP*, purchased from Nanocomp Technologies Inc.) with the nanotube length of hundreds of micrometer. The buckypaper strips were mechanically stretched using a Shimadzu machine (AGS-J, Shimadzu Scientific Inc., Japan) with proper resin assistance, the resulting buckypaper was named as *StrxBP*, *x* is the percentage of the stretching ratio of the buckypaper. The liquid crystalline polymer poly [(benzoyl-1, 4-phenylene)-co-(1, 3-phenylene)] trademarked as Parmax (Mississippi Polymer Technologies Inc), was used to fabricate thermoplastic composites in this work.

4.2. Composite Preparation

Parmax pellets were first dissolved in dimethylformamide (DMF) with the assistance of sonication. The differently stretched buckypapers were impregnated with a Parmax/DMF (0.5 mg ml^{-1}) solution, and then dried at 453 K in a vacuum oven for 12 h to remove residual solvent. The nanotube concentration was controlled around 55 ± 8 wt% (weight loading) in the final buckypaper/Parmax prepreg sheets. The buckypaper prepregs were subjected to a pressure of approximately 2.0 MPa at 563 K for 30 min and then cooled down to room temperature naturally. The samples were named as *StryBPmx* based on the stretching ratio of buckpaper, *y* is the percentage of stretch ratio of the buckypaper in the hybrid composites.

4.3. Characterization

The surface and cross-sectional morphologies of the buckypapers and composites were examined using a field emission scanning electron microscope (JEOL 7401F) with a beam voltage of 10 kV. The nanostructure and the orientation distribution of the differently stretched buckypapers and their composites were investigated by X-ray scattering performed on a Bruker NanoSTAR system with an Incoatec IlS microfocus X-ray source operating at 45 kV and 650 μA. A Cu *Kα* radiation beam ($\lambda = 0.154$ nm) with a beam size about 0.15 mm in full-width half-maximum (FWHM) at the sample position was obtained by collimating the primary beam with cross-coupled Gobel mirrors and a pinhole of 0.1 mm in diameter. A Shimatsu AGS-J materials testing system (Kyoto, Japan) was employed to test the tensile properties of the buckypapers and their thermoplastic composites at room temperature (296 ± 2 K), 40 ± 5% relative humidity, with a crosshead speed of 1 mm min^{-1} on a 500 N load cell with a 25 mm gauge length. The composite strips for tensile tests were cut with dimensions of approximately 50 mm (L) × 5 mm (W) × 20–50 μm (D), and the averaged results were obtained by testing at least five specimens of each composite type to ensure reproducibility. Considering the cross-sectional area decreasing and necking, true stress/strain curves are obtained by the instantaneous load acting on the actual cross-sectional area and assuming material volume remains constant.[37,57] The in-plane electrical and thermal conductivities of the buckypaper/Parmax composites were measured along the stretching direction using the physical property measurement system (PPMS, Quantum Design) with a thermal transport option. The samples with typical thicknesses of 0.05 mm were cut into 10 mm (stretching direction) × 2 mm strips, and the probe distance was about 5 mm. One end of a sample was attached with a resistive heater and a temperature sensor through metal lead using thermally conductive silver epoxy, while the other end was connected to a cold foot and a second temperature sensor. The temperature difference between the two sensors and the dimension were used to calculate the in-plane thermal conductance/conductivity under a given power heating. The heat loss from the heater was minimized by using high vacuum and radiation shields. Afterward, the electrical conductivity of the composite strip was measured at the same temperature with the same two-probe contacts.

Article first published online: May 20, 2016
Manuscript Revised: May 2, 2016
Manuscript Received: March 9, 2016

[1] J. M. Geary, J. W. Goodby, A. R. Kmetz, J. S. Patel, *J. Appl. Phys*. **1987**, *62*, 4100.
[2] A.-M. Vuorinen, S. R. Dyer, L. V. J. Lassila, P. K. Vallittu, *Compos. Interfaces* **2011**, *18*, 387.
[3] J. M. Geary, J. W. Goodby, A. R. Kmetz, J. S. Patel, *J. Appl. Phys*. **1987**, *62*, 4100.
[4] S. Berber, Y. K. Kwon, D. Tomanek, *Phys. Rev. Lett*. **2000**, *84*, 4613.
[5] Q. Zhao, M. B. Nardelli, J. Bernholc, *Phys. Rev. B* **2002**, *65*, 144105.
[6] M.-F. Yu, B. S. Files, S. Arepalli, R. S. Ruoff, *Phys. Rev. Lett*. **2000**, *84*, 5552.
[7] H. G. Chae, S. Kumar, *Science* **2008**, *319*, 908.
[8] Z. Wang, P. Ciselli, T. Peijs, *Nanotechnology* **2007**, *18*, 455709.
[9] H. Krenchal, *Fiber Reinforcement: Theoretical and Practical Investigations of the Elasticity and Strength of Fiber-Reinforced Materials*, Akademisk forlag, Copenhagen **1964**.
[10] F. M. Blighe, K. Young, J. J. Vilatela, A. H. Windle, I. A. Kinloch, L. Deng, R. J. Young, J. N. Coleman, *Adv. Funct. Mater*. **2011**, *21*, 364–371.
[11] J. Rosenthal, *Polym. Compos*. **1992**, *13*, 462.
[12] M. J. Folkes, *Short Fiber Reinforced Thermoplastics, Research Study Press*, Wiley, New York **1982**.
[13] L. Berhan, Y. B. Yi, A. M. Sastry, E. Munoz, M. Selvidge, R. Baughman, *J. Appl. Phys*. **2004**, *95*, 4335.

[14] P. C. Song, C. H. Liu, S. S. Fan, *Appl. Phys. Lett*. **2006**, *88*, 153111.
[15] D. S. Lashmore, *Supercapacitors and Methods of Manufacturing Same*, US Patent No. 20080225464, **2008**.
[16] Q. Cheng, J. Bao, J. G. Park, Z. Liang, C. Zhang, B. Wang, *Adv. Funct. Mater.* **2009**, *19*, 3219.
[17] D. A. Walters, M. J. Casavant, X. C. Qin, C. B. Huffman, P. J. Boul, L. M. Ericson, E. H. Haroz, M. J. O'Connell, K. Smith, D. T. Colbert, R. E. Smalley, *Chem. Phys. Lett*. **2001**, *338*, 14.
[18] K. Jiang, Q. Li, S. Fan, *Nature* **2002**, *419*, 801.
[19] R. Downes, S. Wang, D. Haldane, A. Moench, R. Liang, *Adv. Eng. Mater.* **2015**, *17*, 349.
[20] T. Liu, S. Kumar, *Chem. Phys. Lett*. **2003**, *378*, 257.
[21] Z. Li, R. Downes, Z. Liang, *Macromol. Chem. Phys*. **2015**, *216*, 292.
[22] H. H. Gommans, J. W. Alldredge, H. Tashiro, J. Park, J. Magnuson, A. G. Rinzler, *J. Appl. Phys*. **2000**, *88*, 2509.
[23] E. Anglaret, A. Righi, J. L. Sauvajol, P. Bernier, B. Vigolo, P. Poulin, *Phys. Rev. B* **2002**, *65*, 165426.
[24] J. Vavro, M. C. Llaguno, J. E. Fischer, S. Ramesh, R. K. Saini, L. M. Ericson, V. A. Davis, M. Pasquali, R. E. Smalley, *Phys. Rev. Lett*. **2003**, *90*, 065503.
[25] J. E. Fischer, W. Zhou, J. Vavro, M. C. Llaguno, C. Guthy, R. Haggenmueller, M. J. Casavant, D. E. Walters, R. E. Smalley, *J. Appl. Phys*. **2003**, *93*, 2157.
[26] M. Endo, H. Muramatsu, T. Hayashi, Y. A. Kim, M. Terrones, M. S. Dresselhaus, *Nature* **2005**, *433*, 476.
[27] M. Zhang, S. Fang, A. A. Zakhidov, S. B. Lee, A. E. Aliev, C. D. Williams, K. R. Atkinson, R. H. Baughman, *Science* **2005**, *309*, 1215.
[28] S. Li, J. G. Park, Z. Liang, Th. Siegrist, T. Liu, M. Zhang, Q. Cheng, B. Wang, Ch. Zhang, *Carbon* **2012**, *50*, 3859.
[29] G. Lielens, P. Pirotte, A. Couniot, F. Dupret, R. Keunings, *Compos. A* **1997**, *29*, 63.
[30] J. J. Vilatela, J. A. Elliott, A. H. Windle, *ACS Nano* **2011**, *5*, 1921.
[31] K. Koziol, J. Vilatela, A. Moisala, M. Motta, P. Cunniff, M. Sennett, A. Windle, *Science* **2007**, *318*, 1892.
[32] J. Hone, M. C. Llaguno, N. M. Nemes, A. T. Johnson, J. E. Fischer, D. A. Walters, M. J. Casavant, J. Schmidt, R. E. Smalley, *Appl. Phys. Lett*. **2000**, *77*, 666.
[33] N. G. Sahoo, H. K. F. Cheng, L. Li, S. H. Chan, J. Zhao, *Adv. Funct. Mater.* **2009**, *19*, 3962.
[34] C.-Y. Chang, E. M. Phillips, R. Liang, S. W. Tozer, B. Wang, C. Zhang, Hs.-T. Chiu, *J. Appl. Polym. Sci*. **2013**, *128*, 1360.
[35] L. He, J. Sun, X. Wang, X. Fan, Q. Zhao, L. Cai, R. Song, Z. Ma, W. Huang, *Mater. Chem. Phys*. **2012**, *134*, 1059.
[36] J. Gou, Z. Liang, C. Zhang, B. Wang, *Compos. Part. B Eng*. **2005**, *36*, 524.
[37] R. D. Downes, A. Hao, J. G. Park, Y.-F. Su, R. Liang, B. D. Jensen, E. J. Siochi, K. R. E. Wise, *Carbon* **2015**, *93*, 953.
[38] K. Young, F. M. Blighe, J. J. Vilatela, A. H. Windle, I. A. Kinloch, L. Deng, R. J. Young, J. N. Coleman, *ACS Nano* **2010**, *4*, 6989.
[39] J. N. Coleman, U. Khan, W. J. Blau, Y. K. Gunko, *Carbon* **2006**, *44*, 1624.
[40] T. Mori, K. Tanak, *Acta Metall*. **1973**, *21*, 571.
[41] J. Rosenthal, *Polym. Comp*. **1992**, *13*, 462.
[42] K. Yang, J. He, Z. Su, J. B. Reppert, M. J. Skove, T. M. Tritt, A. M. Rao, *Carbon* **2010**, *48*, 756.
[43] E. S. Choi, J. S. Brooks, D. L. Eaton, M. S. Al-Haik, M. Y. Hussaini, H. Garmestani, D. Li, K. Dahmen, *J. Appl. Phys*. **2003**, *94*, 6034.
[44] L. M. Veca, M. J. Meziani, W. Wang, X. Wang, F. Lu, P. Zhang, Y. Lin, R. Fee, J. W. Connell, Y.-P. Sun, *Adv Mater.* **2009**, *21*, 2088.
[45] C. Stephan, T. P. Nguyen, B. Lahr, W. Blau, S. Lefrant, O. Chauvet, *J. Mater. Res*. **2002**, *17*, 396.
[46] F. H. Gojny, M. H. G. Wichmann, B. Fiedler, I. A. Kinloch, W. Bauhofer, A. H. Windle, K. Schulte, *Polymer* **2006**, *47*, 2036.
[47] S. Pegel, P. Potschke, T. Villmow, D. Stoyan, G. Heinrich, *Polymer* **2009**, *50*, 2123.
[48] Y. L. Li, I. A. Kinloch, A. H. Windle, *Science* **2004**, *304*, 276.
[49] M. S. P. Shaffer, A. H. Windle, *Adv. Mater.* **1999**, *11*, 937.
[50] Q. F. Cheng, J. P. Wang, K. L. Jiang, Q. Q. Li, S. S. Fan, *J. Mater. Res*. **2008**, *23*, 2975.
[51] J. Gou, Z. Liang, C. Zhang, B. Wang, *Compos. Part. B Eng*. **2005**, *36*, 524.
[52] J. E. Fischer, W. Zhou, J. Vavro, M. C. Llaguno, C. Guthy, R. Haggenmueller, M. J. Casavant, D. E. Walters, R. E. Smalley, *J. Appl. Phys*. **2003**, *93*, 2157.
[53] N. G. Sahoo, H. K. F. Cheng, L. Li, S. H. Chan, J. Zhao, *Polym. Adv. Technol*. **2011**, *22*, 1452.
[54] K. Yang, J. He, Z. Su, J. B. Reppert, M. J. Skove, T. M. Tritt, A. M. Rao, *Carbon* **2010**, *48*, 756–62.
[55] J. Hone, M. C. Llaguno, N. M. Nemes, A. T. Johnson, J. E. Fischer, D. A. Walters, M. J. Casavant, J. Schmidt, R. E. Smalley, *Appl. Phys. Lett*. **2000**, *77*, 666.
[56] N. Wakeham, A. F. Bangura, X. Xu, J.-F. Mercure, M. Greenblatt, N. E. Hussey, *Nat. Commun*. **2011**, *2*, 396.
[57] W. D. Callister, D. G. Rethwisch, *Materials Science and Engineering an Introduction*, 7th edition, John Wiley & Sons, Inc., New York, NY **2007**.

